Published in final edited form as:
Nano Lett. 2009 March ; 9(3): 1111–1116. doi:10.1021/nl803548b.

Impact of Order and Disorder in RGD Nanopatterns on Cell Adhesion

Jinghuan Huang[1,2], **Stefan V. Gräter**[2], **Francesca Corbellini**[2], **Sabine Rinck-Jahnke**[2], **Eva Bock**[2], **Ralf Kemkemer**[2], **Horst Kessler**[3], **Jiandong Ding**[*,1], and **Joachim P. Spatz**[*,2]

1 *Key Laboratory of Molecular Engineering of Polymers of Ministry of Education, Department of Macromolecular Science, Advanced Materials Laboratory, Fudan University, Shanghai 200433, China*

2 *Department of New Materials and Biosystems, Max Planck Institute for Metals Research, and Department of Biophysical Chemistry, University of Heidelberg, Heisenbergstrasse 3, D-70569 Stuttgart, Germany*

3 *Center of Integrated Protein Science Munich at the Technical University of Munich, Department Chemie, Technical University of Munich, Lichtenbergstrasse 4, D-85747 Garching, Germany*

Abstract

We herein present a novel platform of well-controlled ordered and disordered nanopatterns positioned with a cyclic peptide of arginine-glycine-aspartic acid (RGD) on a bioinert poly(ethylene glycol) background, to study whether the nanoscopic order of spatial patterning of the integrin-specific ligands influences osteoblast adhesion. This is the first time that the nanoscale order of RGD ligand patterns was varied quantitatively, and tested for its impact on the adhesion of tissue cells. Our findings reveal that integrin clustering and such adhesion induced by RGD ligands is dependent on the local order of ligand arrangement on a substrate when the global average ligand spacing is larger than 70 nm; i.e., cell adhesion is “turned off” by RGD nanopattern order and “turned on” by the RGD nanopattern disorder if operating at this range of inter-ligand spacing.

Integrin plays a central role in the formation of focal adhesions (FAs), which anchor cells to the extracellular matrix (ECM).[1] High-affinity binding of the integrin transmembrane proteins to ECM ligands has been extensively exploited for tailoring artificial synthetic ECM systems.[2] Thus far, it has been reported that cell responses to the synthetic ECM depend to a large extent on multiple substrate features, such as its chemical composition,[3–6] geometry and topographical features,[7] ligand organization,[8,9] and even substrate stiffness.[10,11] In particular, the spatial organization of the integrin-specific peptide sequence of arginine-glycine-aspartic acid (RGD) on non-fouling substrates has attracted much attention. This sequence, contained in many ECM proteins, can be recognized by all five aV integrins (αVβ1, αVβ3, αVβ5, αVβ6, αVβ8), two β1 integrins (α5β1, α8β1) and αIIbβ3.[12] Once ligated, the integrin receptors link the ECM to the cytoskeleton and integrate intracellular and extracellular events. Furthermore, it is known that cellular behaviors such as adhesion, migration, proliferation and differentiation, are quite sensitive to the bioactivity, tether length, interspacing and density of surface RGD ligands in artificial ECM materials.[13–21]

Recent developments in nanotechnology have given access to the nanoscale organization of RGD ligands in both inorganic and polymeric substrates mimicking ECMs. Research concerning randomly dispersed RGD ligands grafted onto polymeric materials suggested that

*Corresponding authors: E-mail: E-mail: Spatz@mf.mpg.de (J.P. Spatz); E-mail: jdding1@fudan.edu.cn (J. Ding).

Supporting Information Available: A detailed description of the experimental protocols for sample preparation and characterization is available free of charge via the Internet at http://pubs.acs.org.

cell adhesion and spreading can be dramatically reduced when the average ligand spacing was beyond ~67 nm[15,16,18,19,22] The precise determination of ligand spacing suffers, however, from difficulties in estimating the surface density from a bulk concentration, and also from the polydispersity of local ligand spacings which is the distance between two adjacent biomolecules. On the other hand, ordered nanopatterning of ligands on non-fouling interfaces by means of newly established micelle nanolithography techniques, has been applied in cell studies.[23–27]

Nevertheless, there has been no report to date of studies comparing cellular responses to nanostructured surfaces characterized by ordered or disordered organization of biomolecules such as RGD ligands. Herein, we chose to examine this critical issue in cell-nanomaterial interactions by exploring osteoblast adhesion regulated by the nanoscale organization of RGD ligands in defined orders. In particular, we investigated how cellular behaviors are influenced by the lateral positioning of single integrin receptors with a series of average interdistances and varied polydispersity of interdistances under a defined particle density.

In this work, both ordered and disordered c(-RGDfK-)-thiol ligand nanopatterns on poly (ethylene glycol) (PEG) interfaces were fabricated. The experimental procedures are schematically depicted in Figure 1. First, ordered and disordered gold (Au) nanopatterns were prepared on glass substrates via the previously reported micelle nanolithography technique, using polystyrene-*block*-poly(2-vinylpyridine) (PS-*b*-P2VP) as the main template polymer.[28,29] In particular, the present paper introduces a modified micellar modulation approach to the fabrication of corresponding disordered Au nanopatterns, involving the addition of homopolymer polystyrene (PS) as an ordering interference reagent. Au nanopatterns were obtained by oxygen plasma treatment of a self-assembled monolayer of micelles loaded with hydrogen tetrachloroaurate ($HAuCl_4$).[30] Subsequently, the area on the glass substrate not covered by Au nanoparticles was covalently grafted with a monolayer of the linear PEG-silane (2-[methoxy(polyethyleneoxy)propyl]trimethoxysilane, namely M-PEG-Si$(OMet)_3$), to prevent nonspecific cell adhesion.[23,31] The adhesive dots for cells were then constructed by coupling c(-RGDfK-)-thiol ligands to Au nanoparticles via the thiol group, so that each nanoparticle could bind up to one integrin. Finally, MC3T3-E1 osteoblasts, known to express several subtypes of integrins (e.g., $\alpha V\beta 3$ and $\alpha V\beta 5$), were utilized, to evaluate cell adhesion on various nanopatterns of c(-RGDfK-)-thiol ligands. As a control, experiments involving cell adhesion to RGE functionalized and non-functionalized Au nanoparticle patterns were conducted. No significant cellular response to such patterns was seen, in agreement with previous findings,[23,24,26] indicating that adhesion is entirely due to the cell's interaction with c(-RGDfK-)-thiol ligand-modified Au nanoparticles.

As a result, the order of nanopatterns could be well-controlled by the addition of PS homopolymer as an ordering interference reagent. The ratios of PS/PS-*b*-P2VP were altered to adjust the spatial order, while avoiding either the aggregation or the distortion of micelles. The interparticle distance or particle density of nanopatterns was modulated by varying the preparation conditions, such as the molecular weight of PS-*b*-P2VP, the concentration of the micelle solution, and the pulling speed of substrates during dip-coating.[26,28,29] Moreover, the diameter of the Au nanoparticles was adjusted by varying the loading amount of the metal precursor $HAuCl_4$ in the micelles. Au nanopatterns with defined orders and sizes were produced by means of dip-coating and subsequent plasma etching. The samples were characterized by atomic force microscopy (AFM). The image data were statistically processed by a self-designed program to obtain values such as the order parameters as defined in the Supporting Information. As shown in Table 1, the resulting nanopatterns, with and without addition of the homopolymer, exhibited significantly different order parameters. Figure 2a–h shows representative AFM images of ordered and disordered Au nanopatterns on glass substrates, with average interparticle distances varying from 55 to 101 nm.

A typical AFM image of a nanopattern after PEG- passivation and RGD-coupling is shown in Figure 3a. This treatment also influenced the height of the Au nanoparticles and the global wetting behavior of the surface, as shown in Figure 3b and c. After passivation, a smooth PEG layer with a thickness of ~2.3 nm was formed on the glass surface. The contact angle of water against differently prepared glass surfaces increased from 4.6 ± 1.3° to 35.3 ± 0.8° and 35.2 ± 0.6° (for nanopatterned and non-nanopatterned regions, respectively). The functionalization of c(-RGDfK-)-thiol ligands to Au nanoparticles resulted in a ~2.1 nm increase in particle height, and a slight drop of contact angle to 34.7 ± 0.9°. Furthermore, the borderline (the so-called "dipping line" formed during the dip-coating process) between the nanopatterned region and the non-nanopatterned region was clearly delineated by cells adhering to the surface even after 48 h in culture (Figure 3d), illustrating the success of PEG-passivation and subsequent RGD-coupling.

In this work, the RGD-adhesive particles in the final ligand nanopatterns were slightly above 10 nm in height. Since the diameter of an integrin is approximately 8–12 nm,[32] each RGD-adhesive particle provides an individual anchoring site for a single integrin to bind. In principle, one integrin binds specifically to only one c(-RGDfK-)-thiol ligand. Once occupied by an integrin, the anchoring site will be inaccessible to neighboring integrins due to steric hindrance. Furthermore, since the spacer between the c(-RGDfK-)-thiol and the Au nanoparticle is ~2 nm, the diffusion amplitude of the immobilized c(-RGDfK-)-thiol ligand is estimated to be less than 1 nm. Hence, the spatial arrangement of the original Au nanopatterns well reflects the c(-RGDfK-)-thiol ligand lattice, and thus the final lateral positioning of integrins, which may trigger focal adhesion formation.

In the next step, cell adhesion experiments were performed with MC3T3-E1 osteoblasts on ordered and corresponding disordered c(-RGDfK-)-thiol ligand nanopatterns. Micrographs of fluorescently labeled cells were taken after 24 h in culture, as shown in Figure 4a–h. The number of adherent cells per unit area and the average projected area per cell were statistically quantified to correlate with the ligand order as well as the inter-ligand distance (Figure 4i, j).

In the case of ordered c(-RGDfK-)-thiol ligand nanopatterns, when the average inter-ligand spacing increased from 55 to 100 nm, and the ligand density decreased from 413 ± 6 to 118 ± 9 μm^{-2}, a remarkable change in MC3T3-E1 osteoblast morphology was observed, from well-spread to a spike-like shape, and eventually to a highly elongated shape (Figure 4a–d). Especially on ordered 94 nm- and 100 nm-spaced nanopatterns, only a small fraction of attached cells could be seen. In contrast, only slight variations in cell morphology and density could be found on disordered nanopatterns (Figure 4e–h). Even if the average inter-ligand spacing increased beyond 92 nm, a number of well-spread cells could still be observed.

A significant change in the number of adherent cells was also revealed by statistical analysis. On the ordered ligand nanopatterns, as inter-ligand spacing increased, both the number of adherent cells and the projected cell area dropped sharply, from ~192 to ~56 mm^{-2} and from ~2840 to ~1760 μm^2/cell, respectively. On the corresponding disordered ligand nanopatterns, relatively weak changes were observed, from ~199 to ~97 mm^{-2} and from ~2930 to ~2570 μm^2/cell, respectively. Hence, the disordered nanopatterns provide a much greater variety of ligand densities for positive cell adhesion.

To further demonstrate the different types of osteoblast adhesion on ordered and disordered RGD nanopatterns, fluorescent immunostaining experiments were performed. The intracellular proteins actin and vinculin, generally involved in FA formation, were fluorescently labeled and monitored by high magnification microscopy, as shown in Figure 5. In agreement with Figure 4, despite the morphological changes in cells due to variations in the global average inter-ligand spacing, cells plated on disordered ligand nanopatterns spread

significantly more effectively than those on the ordered ligand nanopatterns if the average ligand spacing in the former or the latter instance was larger than 70 nm. Thicker filamentous actin bundles were observed in cells growing on disordered ligand nanopatterns, compared to the corresponding ordered ones (Figure 5A). Vinculin denotes the locations of FA, to a certain extent. As shown in Figure 5B, throughout the varied range of global average inter-ligand spacing, considerably stronger expression and defined clustering of vinculin in cells plated on disordered samples were seen, while those on ordered samples were relatively weak except for the 55 nm-spaced nanopattern.

In the case of quasi-hexagonal ordered ligand nanopatterns, cell adhesion revealed a strong dependence on the average inter-ligand spacing (Figures 4 and 5). A critical ligand spacing of ~70 nm (a global ligand density of ~231 μm^{-2}) was revealed, above which cell attachment and spreading were highly restricted. This value is quite consistent with previous findings, and is typical for many cell types.[23,24,26] Notably, the average global inter-ligand spacing well represents the actual local ligand spacings in ordered nanopatterns, due to their relative monodispersity. The negative cellular response to ligand spacings beyond ~70 nm is ascribed to a lack of effective integrin clustering, inhibiting the formation of stable FAs and actin fiber networks, as schematically presented in Figure 6. In principle, integrins in the cell membrane could still be activated by c(-RGDfK-)-thiol ligands with > ~70 nm spacings, via the specific anchoring junction. In the case of overly large interdistances, however, subsequent integrin interaction is restricted. By observing cell behavior on an ordered nanopattern, Cavalcanti-Adam et al. found that overlarge inter-ligand spacing significantly delayed cell spreading and protrusion-retraction cycles.[24] Recently, it was also hypothesized that the cellular adhesion apparatus has its own internal periodicity of 67 nm.[22] The dimension fits well with the molecular sizes of α-actinin or talin which fall within ca. 60 nm.[33] To some extent, cells may adjust this periodicity to fit the extracellular binding sites.[26] As schematically shown in Figure 6, we propose that a critical lateral distance appears, due to the requirement of lateral crosslinking of intergins by proteins such as α-actinin or talin. In either case, effective integrin clustering is required, following activation of the integrin via RGD binding. Hence, a critical interdistance of RGD functionalized Au nanoparticles becomes key to an effective outside-in transduction signal. The fabrication of ordered and disordered nanopatterns, suggested for the first time in the present study, provides an excellent tool to study this view, as nanopatterns that are merely ordered with a series of interdistances, cannot decouple global RGD density and local intermolecular spacing.[23,27] Results from random coating or grafting of ligands are less deterministic and may not help in answering the role of inter-biomolecule separation on cell adhesion. Our results indicate that the effect of order degree is not significant if the interdistance of RGD ligands is less than 70 nm. However, Figure 4 and 5 reveal much difference between cell adhesion on ordered and disordered nanopatterned surfaces, when the average inter-ligand spacing exceeds 70 nm. Given that an FA can only be formed when the local spacings of underlying integrins are below 70 nm, we presume that the integrins could be divided into two classes, clustering and non-clustering (Figure 6c,d; denoted by black disks and white disks, respectively). Here, an integrin is defined to be in a “cluster” if the distance between this integrin and its nearest neighboring integrin is less than the critical ligand spacing; i.e., 70 nm. Lately, the critical number of activated intergins with a lateral spacing of less than 70 nm, which enables FA formation, was determined to be six per adhesion site which supports the point of view that local clustering of integrins is mandatory for stable adhesion formation.[27] The average inter-ligand spacing is directly equivalent to local inter-ligand spacing, only in ordered nanopatterns. Due to polydispersity, a disordered nanopattern clearly leads to more integrin clustering (Figure 6c) than a corresponding ordered one, when the global average interdistance is above the critical ligand spacing..

In conclusion, both ordered and disordered c(-RGDfK-)-thiol ligand nanopatterns on PEG-passivated supports were successfully fabricated for the lateral positioning of integrins as single

adhesion receptors in defined orders and spacings in cell adhesion processes. The osteoblast adhesion quality on these substrates were examined in a comparative manner and proved that order in adhesive nanopattern matters if local ligand-ligand spacing is > 70 nm. By decoupling RGD density and molecularly defined interdistance of biomolecules, we first confirmed the existence of a critical local inter-ligand spacing of ~70 nm, above which cell adhesion was strongly reduced. Second, compared to the ordered ligand nanopattern, the disordered partner provided a much wider range of variation in local inter-ligand spacing for positive cell adhesion, which is due to the polydispersity of local inter-ligand spacings. Therefore, stable adhesion of osteoblasts on disordered nanopattern surfaces is activated at less global adhesion ligand density than it is possible on ordered once.

Supplementary Material

Refer to Web version on PubMed Central for supplementary material.

Acknowledgements

The group from the Fudan University was supported by grants from the Chinese Ministry of Science and Technology (973 Projects No. 2009CB930000 and No. 2005CB522700), the National Science Foundation of China (Grants No. 50533010, No. 20574013, and No. 20774020), the Chinese Ministry of Education (Key Grant No. 305004), Science and Technology Developing Foundation of Shanghai (Grant No. 07JC14005), and the Shanghai Education Committee (Project No. B112). The German group was financially supported by the Landesstiftung Baden-Württemberg and the Max Planck Society. This publication and the project described herein were also partly supported by the National Institutes of Health, through the NIH Roadmap for Medical Research (PN2 EY 016586). We also thank Peptides International, Inc. (USA) for the synthesizing of the c(-RGDfK-)-thiol peptide. JPS holds a Weston Visiting Professorship at the Weizmann Institute of Science.

References

1. Geiger B, Bershadsky A, Pankov R, Yamada KM. Nat Rev Mol Cell Biol 2001;2(11):793–805. [PubMed: 11715046]
2. García AJ. Biomaterials 2005;26(36):7525–7529. [PubMed: 16002137]
3. Keselowsky BG, Collard DM, García AJ. Biomaterials 2004;25(28):5947–5954. [PubMed: 15183609]
4. Kantlehner M, Schaffner P, Finsinger D, Meyer J, Jonczyk A, Diefenbach B, Nies B, Hölzemann G, Goodman SL, Kessler H. Chem BioChem 2000;1(2):107–114.
5. Lieb E, Hacker M, Tessmar J, Kunz-Schughart LA, Fiedler J, Dahmen C, Hersel U, Kessler H, Schulz MB, Göpferich A. Biomaterials 2005;26(15):2333–2341. [PubMed: 15585236]
6. Salber J, Gräter S, Harwardt M, Hofmann M, Klee D, Dujic J, Huang J, Ding J, Kippenberger S, Bernd A, Groll J, Spatz JP, Möller M. Small 2007;3(6):1023–1031. [PubMed: 17455182]
7. Chen CS, Mrksich M, Huang S, Whitesides GM, Ingber DE. Science 1997;276(5317):1425–1428. [PubMed: 9162012]
8. Auernheimer J, Dahmen C, Hersel U, Bausch A, Kessler H. J Am Chem Soc 2005;127(46):16107–16110. [PubMed: 16287297]
9. Irvine DJ, Hue KA, Mayes AM, Griffith LG. Biophysical Journal 2002;82(1):120–132. [PubMed: 11751301]
10. Discher DE, Janmey P, Wang YL. Science 2005;310(5751):1139–1143. [PubMed: 16293750]
11. Engler AJ, Sen S, Sweeney HL, Discher DE. Cell 2006;126(4):677–689. [PubMed: 16923388]
12. Humphries JD, Byron A, Humphries MJ. Journal of Cell Science 2006;119(19):3901–3903. [PubMed: 16988024]
13. Kalinina S, Gliemann H, López-García M, Petershans A, Auernheimer J, Schimmel T, Bruns M, Schambony A, Kessler H, Wedlich D. Biomaterials 2008;29(20):3004–3013. [PubMed: 18433862]
14. Maheshwari G, Brown G, Lauffenburger DA, Wells A, Griffith LG. Journal of Cell Science 2000;113 (10):1677–1686. [PubMed: 10769199]
15. Lee KY, Alsberg E, Hsiong S, Comisar W, Linderman J, Ziff R, Mooney D. Nano Letters 2004;4(8): 1501–1506.

16. Kong HJ, Hsiong S, Mooney DJ. Nano Letters 2007;7(1):161–166. [PubMed: 17212457]
17. Schense JC, Hubbell JA. The Journal of Biological Chemistry 2000;275(10):6813–6818. [PubMed: 10702239]
18. Koo LY, Irvine DJ, Mayes AM, Lauffenburger DA, Griffith LG. Journal of Cell Science 2002;115 (7):1423–1433. [PubMed: 11896190]
19. Massia SP, Hubbell JA. The Journal of Cell Biology 1991;114(5):1089–1100. [PubMed: 1714913]
20. Kuhlman W, Taniguchi I, Griffith LG, Mayes AM. Biomacromolecules 2007;8(10):3206–3213. [PubMed: 17877394]
21. Au A, Boehm CA, Mayes AM, Muschler GF, Griffith LG. Biomaterials 2007;28(10):1847–1861. [PubMed: 17222453]
22. Poole K, Khairy K, Friedrichs J, Franz C, Cisneros DA, Howard J, Mueller D. J Mol Biol 2005;349 (2):380–386. [PubMed: 15890202]
23. Arnold M, Cavalcanti-Adam EA, Glass R, Blümmel J, Eck W, Kantlehner M, Kessler H, Spatz JP. Chem Phys Chem 2004;5(3):383–388. [PubMed: 15067875]
24. Cavalcanti-Adam EA, Volberg T, Micoulet A, Kessler H, Geiger B, Spatz JP. Biophysical Journal 2007;92(8):2964–2974. [PubMed: 17277192]
25. Graeter SV, Huang J, Perschmann N, López-García M, Kessler H, Ding J, Spatz JP. Nano Letters 2007;7(5):1413–1418. [PubMed: 17394372]
26. Arnold M, Hirschfeld-Warneken VC, Lohmüller T, Heil P, Blümmel J, Cavalcanti-Adam EA, López-García M, Walther P, Kessler H, Geiger B, Spatz JP. Nano Letters 2008;8(7):2063–2069. [PubMed: 18558788]
27. Arnold M, Schwieder M, Blümmel J, Cavalcanti-Adam EA, López-García M, Kessler H, Geiger B, Spatz JP. Soft Matter. 200910.1039/b815634d
28. Spatz JP, Sheiko S, Möller M. Macromolecules 1996;29(9):3220–3226.
29. Spatz JP, Herzog T, Mößmer S, Ziemann P, Möller M. Adv Mater 1999;11(2):149–153.
30. Glass R, Arnold M, Blümmel J, Küller A, Möller M, Spatz JP. Adv Funct Mater 2003;13(7):569–575.
31. Blümmel J, Perschmann N, Aydin D, Drinjakovic J, Surrey T, López-García M, Kessler H, Spatz JP. Biomaterials 2007;28:4739–4747. [PubMed: 17697710]
32. Xiong JP, Stehle T, Zhang R, Joachimiak A, Frech M, Goodman SL, Arnaout MA. Science 2002;296 (5565):151–155. [PubMed: 11884718]
33. Meyer RK, Aebi U. The Journal of Cell Biology 1990;110(6):2013–2024. [PubMed: 2351691]

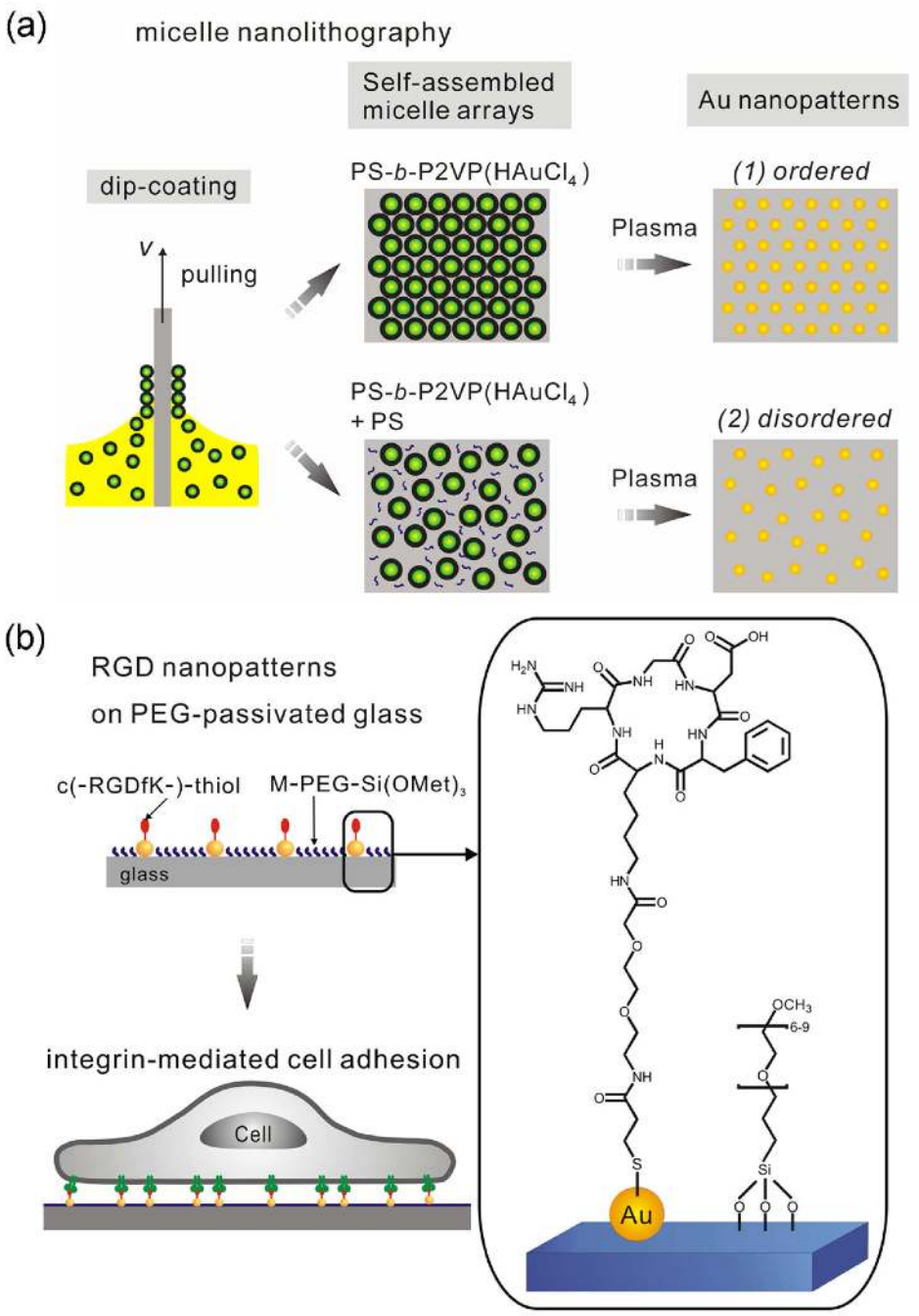

Figure 1.

Schematic presentation of surface-nanopattern preparation for cell adhesion studies. (a) Micelle nanolithography technique for making ordered (*1*) and disordered (*2*) Au nanopatterns on glass surfaces. Here, PS homopolymers were used as an ordering-interference reagent. (b) Fabrication of ligand nanopatterns on PEG-passivated glass. The glass surface was grafted with M-PEG-Si(OMet)$_3$ as a self-assembled monolayer to prevent cell adhesion. Then the protruding Au nanoparticles were biofunctionalized with c(-RGDfK-)-thiol ligands. Subsequently, cell adhesion behaviors on the resulting RGD-nanopatterned surfaces were examined.

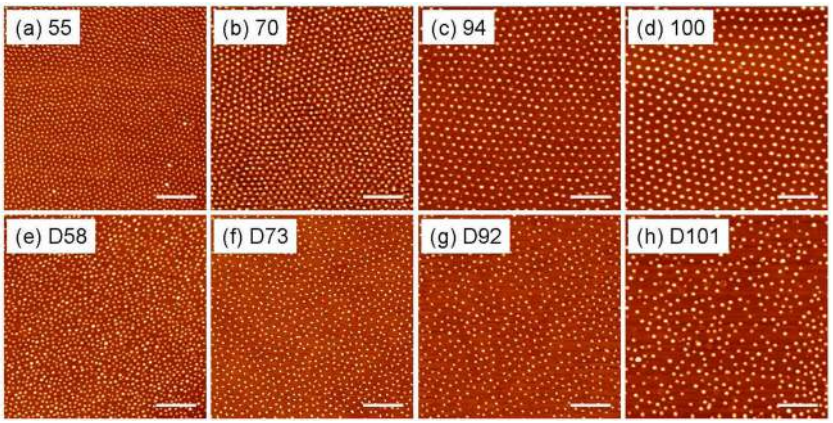

Figure 2.
AFM images of corresponding ordered (a,b,c,d) and disordered (e,f,g,h) gold nanopatterns on glass substrates. Samples are labeled at the top left of each image with the numbers representing the average interparticle distances summarized in Table 1. Scale bars: 400 nm.

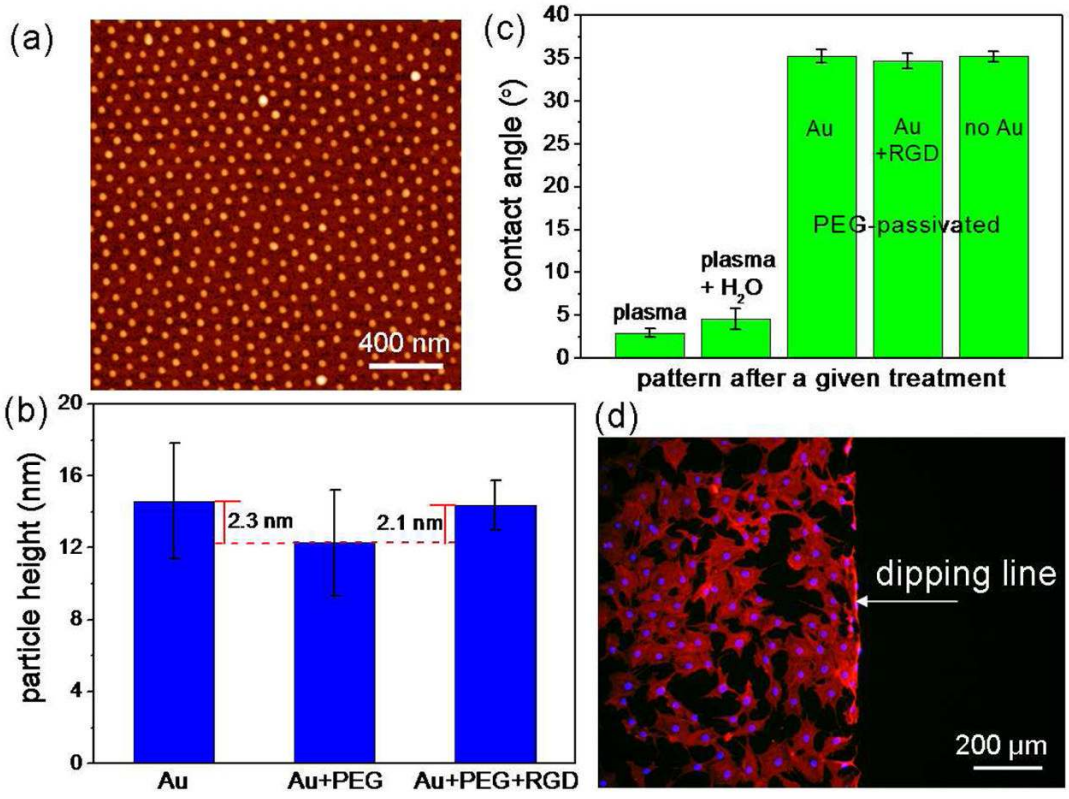

Figure 3.

(a) An AFM image of an Au nanopattern (ordered 112 nm-spaced) with Au nanoparticles coupled with c(-RGDfK-)-thiol ligands. (b) Particle height of nanopatterns, tracing the preparation process: the original Au nanopattern (ordered 112 nm-spaced), a PEG-passivated nanopattern and a PEG-passivated plus RGD-functionalized nanopattern. (c) Surface contact angles yielded by the different surface preparation process. (d) A fluorescent micrograph of MC3T3-E1 osteoblasts stained for actin (red) and nuclei (blue) after 48 h in culture, on an ordered 42 nm-spaced ligand nanopattern. The borderline between the RGD region (left) and the non-nanopatterned region (right) was clearly marked by adhering cells.

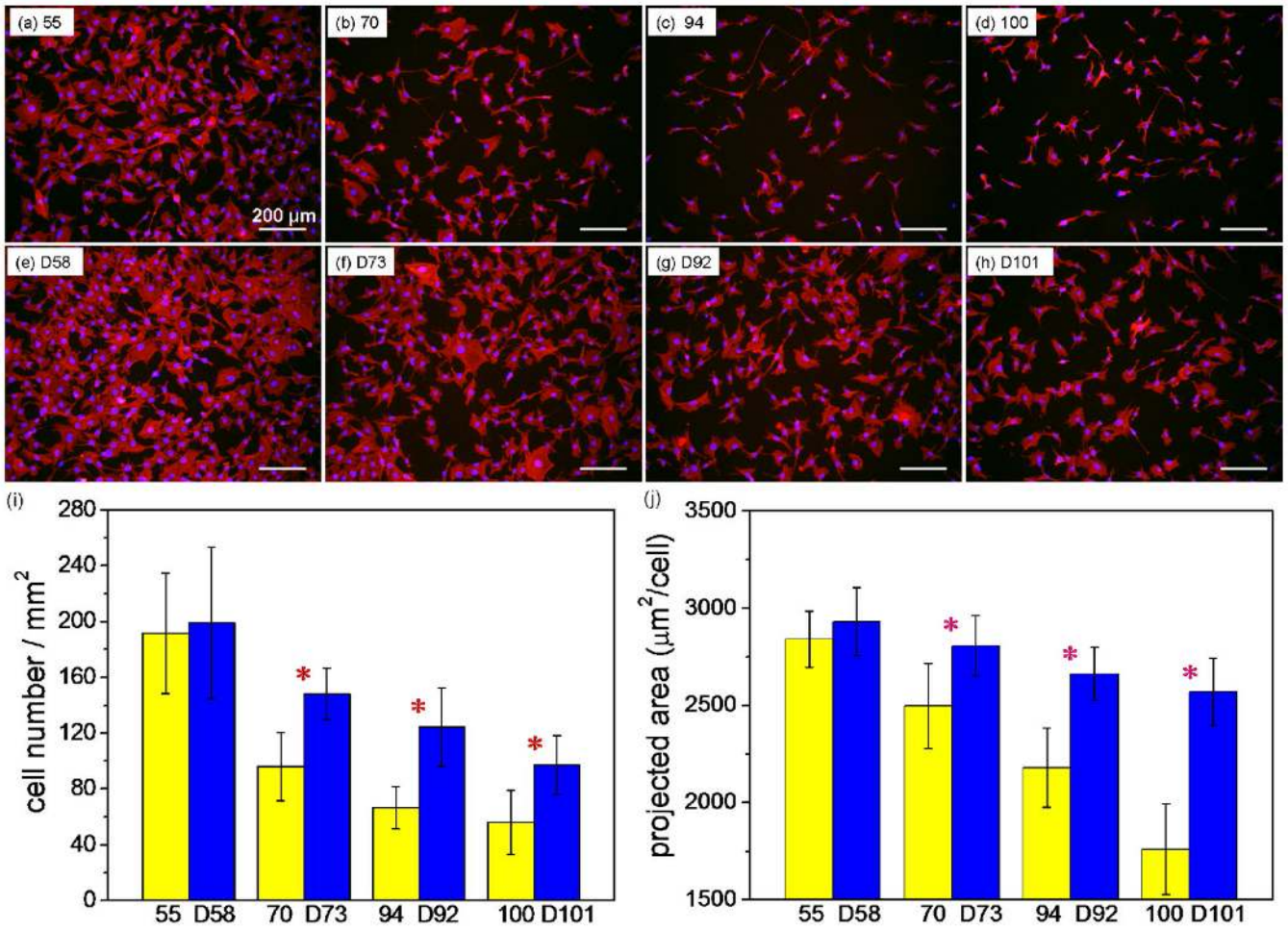

Figure 4.

(a–h) Fluorescent micrographs of MC3T3-E1 osteoblasts labeled for actin (red) and nuclei (blue) after 24 h in culture on ordered (a–d) and disordered (e–h) ligand nanopatterns. All the supports for Au nanopatterns used here were PEG-passivated and the Au particles coupled with c(-RGDfK-)-thiol ligands. Specific nanopatterns are labeled at the top left of each image, with the numbers representing the average inter-ligand distances. (i) Number of cells attached per unit area and (j) projected cell area. An unpaired Student's *t*-test was carried out to compare these results ($n = 12$), with $p < 0.05$ as the criterion of significant difference. Asterisks denote statistical significance from ordered and disordered nanopatterns with similar interparticle distances. Significant differences were also found between any two of the ordered patterns except for 94 and 100, and between any two of the disordered patterns in (i). Significant differences were found between any two of the ordered patterns, and between D73 and either D92 or D101, for the disordered patterns in (j).

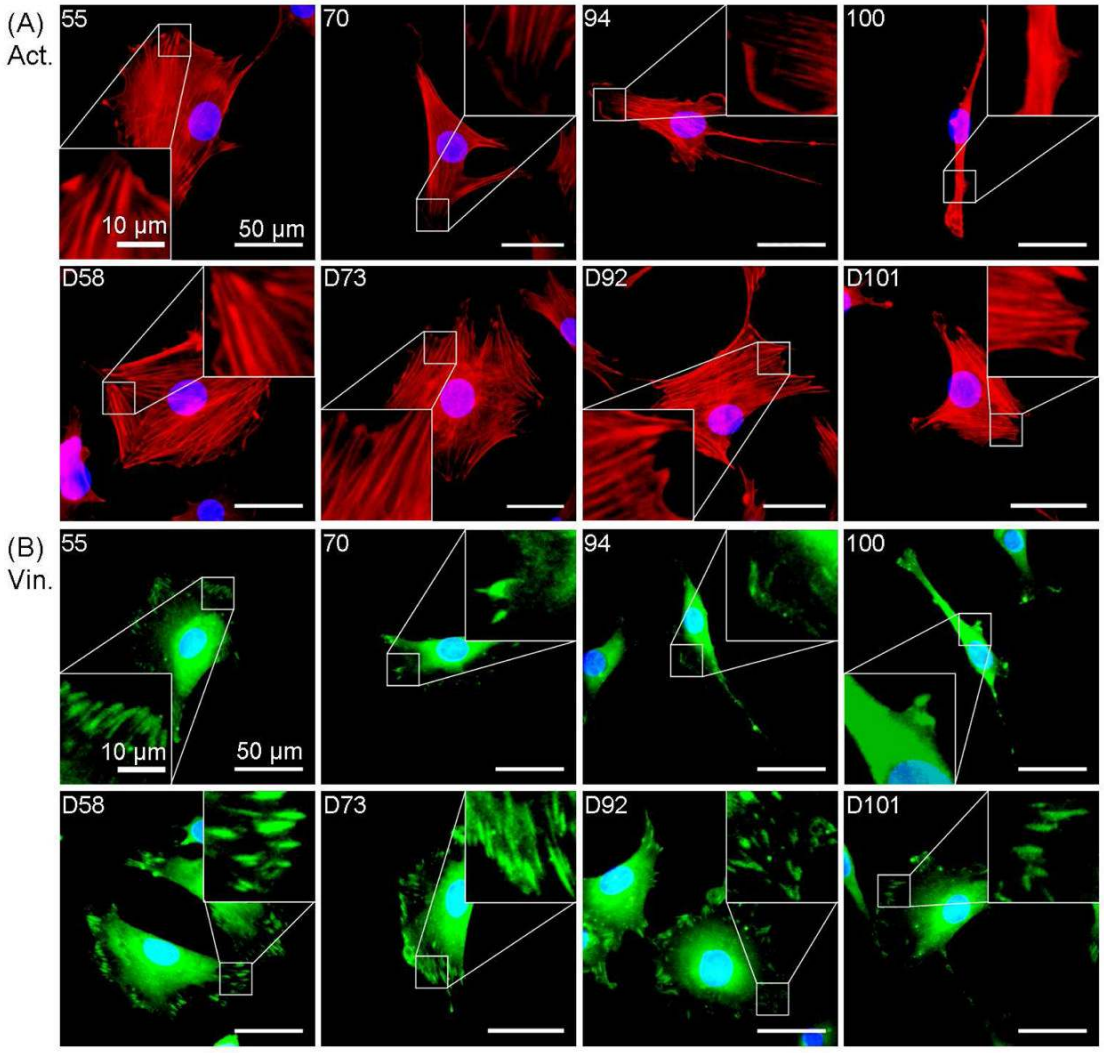

Figure 5.

High-magnification fluorescent micrographs indicating the distributions of actin (A, red), vinculin (B, green) and nuclei (blue) in typical cells. The inset at the top right of each image shows the magnified portion of the cellular structures. Here, MC3T3-E1 osteoblasts were cultured for 24 h on ordered and disordered RGD-adhesive nanopatterns, in parallel with the work presented in Figure 4. Specific nanopatterns are labeled at the top left of each image, with the numbers representing the average inter-ligand distances.

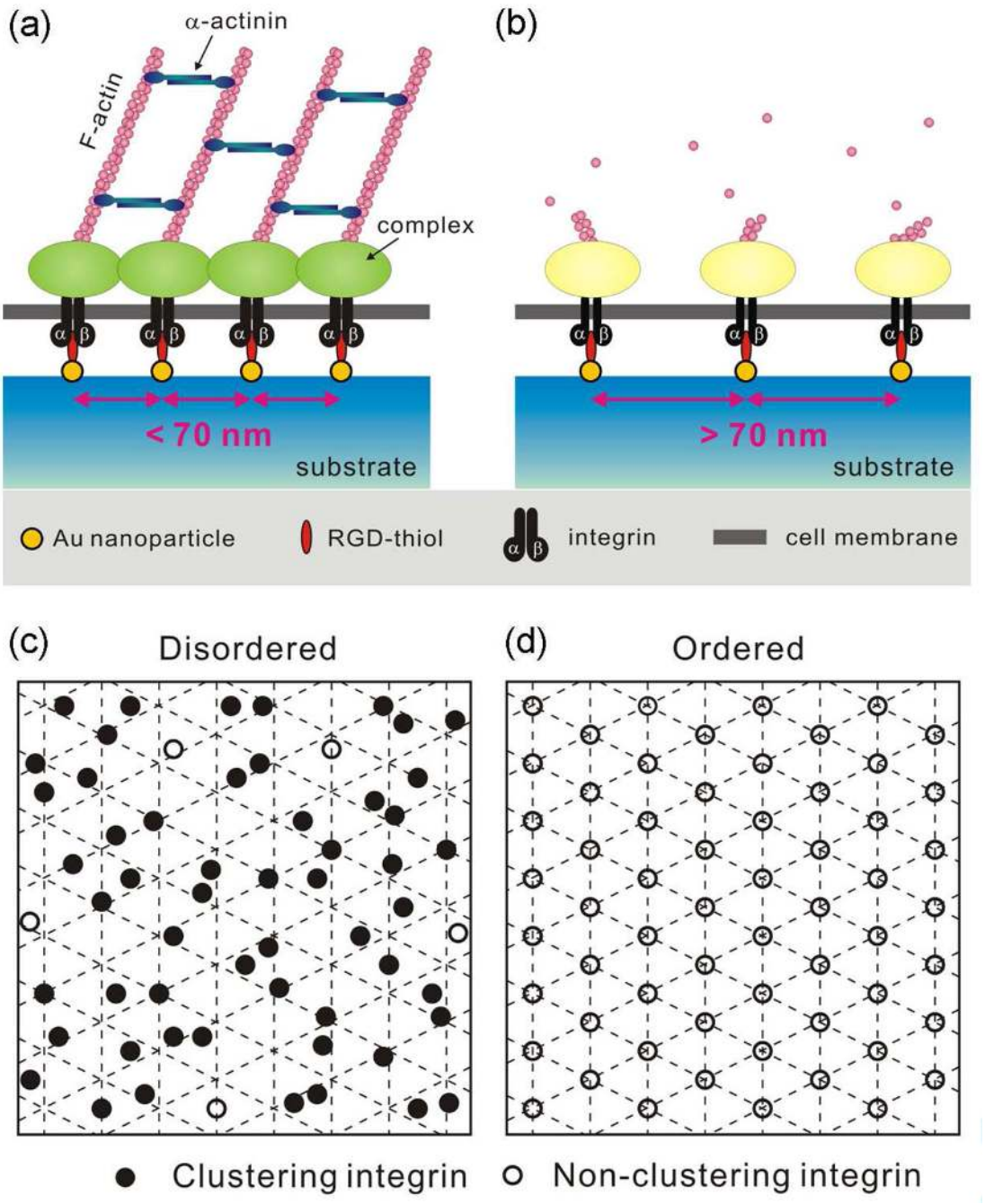

Figure 6.

Sketch of integrin clustering and subsequent focal adhesion formation regulated by different c(-RGDfK-)-thiol ligand nanopatterns. The spatial arrangement of the original Au nanopatterns well reflects the c(-RGDfK-)-thiol ligand lattice and thus, the final lateral positioning of single integrins during cell adhesion. (a) A spacing of < 70 nm between two neighboring c(-RGDfK-)-thiol ligands results in effective integrin clustering and focal adhesion complex formation, followed by the formation of the F-actin cytoskeletal network (only some of the intracellular molecules were depicted here). (b) In contrast, a spacing of > 70 nm, as such, results in neither integrin clustering nor FA complex formation. (c, d) It was presumed that all integrins that potentially bind c(-RGDfK-)-thiol ligands over each nanopattern could be classified as

clustering integrins (black disks); non-clustering integrins (white disks) resulted from interdistances above a critical value. Even at a global average inter-ligand spacing of >70 nm, a disordered nanopattern still displayed some clustering integrins, which was not the case for ordered patterns with inter-ligand spacings of >70 nm.

Table 1

Basic characteristics of ordered/disordered surface nanopatterns

Au nanopatterns	Interparticle distance (nm)[c]	Order parameter[d]	Particle density (particles/μm^2)	Particle diameter (nm)
55[a]	54.9 ± 8.4[e]	0.395 ± 0.168[e]	413 ± 6[e]	10.5 ± 2.1[e]
70	70.3 ± 11.1	0.510 ± 0.066	231 ± 5	8.7 ± 1.3
94	93.6 ± 14.2	0.446 ± 0.153	135 ± 6	15.0 ± 1.4
100	99.8 ± 13.7	0.529 ± 0.122	118 ± 9	15.0 ± 1.4
D58[b]	58.3 ± 13.2	0.125 ± 0.043	362 ± 45	10.4 ± 1.6
D73	73.1 ± 14.6	0.155 ± 0.055	232 ± 9	10.0 ± 1.6
D92	91.9 ± 20.8	0.121 ± 0.046	145 ± 11	10.4 ± 1.7
D101	101.4 ± 25.7	0.120 ± 0.044	117 ± 21	13.5 ± 2.7
42	41.6 ± 9.4	0.384 ± 0.179	685 ± 16	8.9 ± 0.5
112	112.2 ± 16.6	0.358 ± 0.171	92 ± 18	14.6 ± 3.2

[a] Abbreviation of ordered Au nanopatterns with an average interparticle distance of 55 nm.

[b] Abbreviation of disordered Au nanopatterns with an average interparticle distance of 58 nm.

[c] Global average center-to-center distance of nearest neighboring Au nanoparticles.

[d] Degree of order calibrated via a sixfold bond-orientational order parameter.

[e] Mean standard deviation.